ResearchGate

See discussions, stats, and author profiles for this publication at: https://www.researchgate.net/publication/323496910

Optical Microsystem in silicon with CMOS photodiodes optical filters and microlenses

Conference Paper · August 2016

CITATIONS
0

READS
116

5 authors, including:

Yuri Olivato
University of São Paulo
20 PUBLICATIONS **38** CITATIONS

SEE PROFILE

Talita Conte Granado
University of São Paulo
19 PUBLICATIONS **26** CITATIONS

SEE PROFILE

Daniel Ricardo Celino
University of São Paulo
20 PUBLICATIONS **40** CITATIONS

SEE PROFILE

J.H. Correia
University of Minho
446 PUBLICATIONS **3,923** CITATIONS

SEE PROFILE

Some of the authors of this publication are also working on these related projects:

Photonic module NBI for endoscopic capsules View project

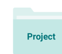
Brain-Lighting View project

All content following this page was uploaded by Daniel Ricardo Celino on 25 March 2018.

The user has requested enhancement of the downloaded file.

Optical microsystem in silicon with CMOS photodiodes, optical filters and microlenses

Y. A. O. Assagra, T. C. Granado, D. R. Celino, J. H. Correia[ξ], J. P. Carmo
University of São Paulo (USP), Dept of Electrical Engineering (SEL), BRAZIL
[ξ]MEMS-UMinho R&D Centre, University of Minho, Dept of Industrial Electronics, PORTUGAL
yuriolivato@gmail.com, jcarmo@sc.usp.br

Abstract—**This paper presents an optical sensor for spectroscopy based on Fabry-Perot interferometry. The components include a CMOS image sensor, microlenses and optical filters for operation in the visible region (e.g., from 480 to 700 nm) of the electromagnetic spectrum. An array of microlenses (made with AZ4562 photoresist material) improves the light impinged into the photodetectors. The on-semiconductor 0.7μm CMOS process was selected for fabricating a microdevice prototype, containing an array of photodetectors. The optical filters were designed for selecting the wavelengths for detection and are made with mirrors based on successive layers of dielectric materials. A prototype based on commercial off-the-shelf components was built and used with a high-gain transresistance amplifier (for photocurrent-to-voltage conversion) for displaying the reading.**

Keywords: **Microlenses, Optical filters, CMOS, photodetectors.**

I. Introduction

It is not stranger the huge range of applications using light spectroscopy because there is no need of physical contact with the analysed sample [1]. By definition, the spectroscopy studies the interaction of light with matter as a function of an individual or a range of wavelengths [2], where the state of electrons can as follows. This will produce one or more effects: scattering, emission or absorption of light. The spectrography is a well established technique that can be found on a broad range of applications/wavelengths: for example on museology/X-Rays [3], steroids detection/UV [4], industrial inspection of product defects/visible range [5], biochemical analysis/visible range [6], quality control for the food industry/visible range [7] and fat content analysis/NIR [8]. The advances of microelectronics industry observed in the last two decades resulted on new and innovative applications, including solid-state circuits (in the digital, mixed-mode and radio-frequency forms), microsensors (e.g., magnetic, displacement, optics) and microactuators (e.g., accelerometers, resonators). In this sense, the optical sensors are the one that benefited with the developments observed in the microelectronic's field [9-10]. The exponential proliferation of CMOS technology and the wide number of optical applications based on this technology clearly proofs this statement [11]. In this sequence of ideas, the application of Multi-Chip-Module (MCM) techniques at the chip level (for joining heterogenic technologies and techniques to obtain compact microsystems with reduced dimensions) pushes this concept further. The microspectrometer is composed by optical filters, microlenses and an image sensor (whose pixels act as individual photodetectors for the individual wavelength channels) for spectroscopy in the visible-range.

II. Design and fabrication

A. Microspectrometer's architecture

The most promising approach for microspectrometers is using an interferometer in conjunction with the microelectronics. Additionally, the most suitable interferometer for dispersing the light and at the same time easy to integrate into the mycrosystem is the Fabry-Perot type, whose principle of operation is illustrated in the Figure 1(a). This is true because the interferometer can be mounted on top of microelectronic devices using IC-compatible fabrication techniques (deposition techniques of both dielectric resonating cavity and mirrors). It must be noted that the mirrors can be made of dielectric and metal layers. Ideally, the output beam contains the ideal peak $\lambda=d/2$. The Figure 1(b) illustrates the complete microsystem that forms the microspectrometer presented in this paper, where it is possible to observe the optical filters, microlenses and an image sensor on CMOS technology (whose pixels act as individual photodetectors for the individual wavelength channels) for spectroscopy in the visible-range.

B. Microlenses

Basically, refractive microlenses are used for collimation, focusing or imaging and are an appealing alternative for applications where miniaturization and alignment simplicity are requirements. A fabrication process based in the thermal reflow was developed for mounting microlenses on top of optical Microsystems composed by optical detectors and filters. As illustrated in Figure 1(b), the microlenses maximize the light impinging into the photodetectors and at the same time reducing the crosstalk between adjacent photodetectors.

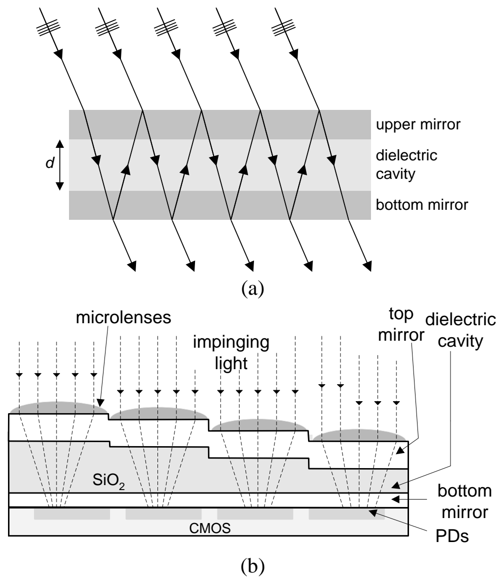

Figure 1: (a) Principle behind the Fabry-Perot interferometry, and (b) an artwork illustrating the several parts of the microspectrometer.

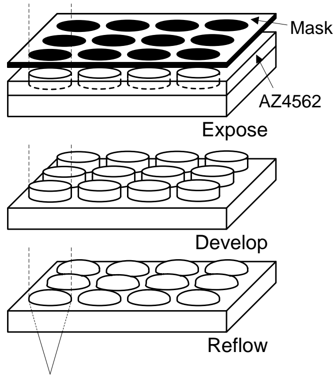

Figure 2: Microlenses array fabrication steps.

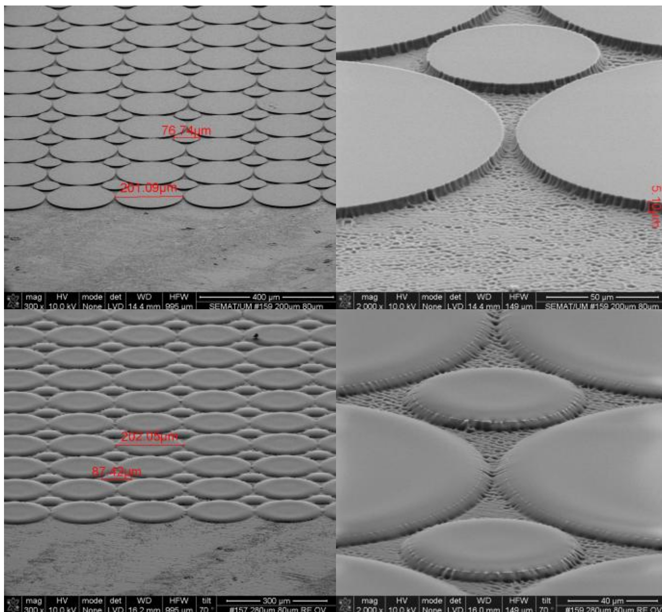

Figure 3: SEMs of few functional prototypes before (on top) and after (on bottom) using the reflow process.

The Figure 2 illustrates the fabrication steps used for fabricating microlenses. In the first step, arrays of strips with circular shape are patterned using a conventional lithography process. In the second step, the strips are subjected to a reflow process. This second step consists on heating the strips until becoming viscous in order to give origin to surface tensions, making the material to reflow and forming a surface with the desired lenticular shape. Different sized arrays were designed and printed into a chromium mask. The AZ4562 photoresist was selected due to the fabrication requirements. This positive photoresist is ideal for coating thicknesses above 3-5 µm without having to increase the exposure energy considerably and still providing enough energy down to the substrate of the AZ4562 material. The Figure 3 shows few functional prototypes, whereas the Table I lists the fabrication process steps and the parameters.

Table I: Microlenses array fabrication process steps and parameters

Process steps	Process parameters
Spin coating	20 second @ 6000 RPM
Prebake (hotplate)	5 minutes @ 100 ºC
Exposure 365 nm (mask aligner)	30 second with the mask aligner in contact mode @ 134 W
Developing	AZ400K or AZ351B developers in a 1:4 concentration with distilled water (2×2min.15secs)
Cleaning	Rinse with distilled water and dry with N_2 flow
Thermal Reflow (hotplate)	5 minutes @ 130ºC

C. *Optical filters (Fabry-Perot cavities)*

The optical filters are key-elements for a good wavelength selection/selectivity and for this reason, dielectric materials were selected. The deposition of successive layers of thin-films is the common method to fabricate optical filters with a given wavelength. For each selected wavelength, the thin-films are designed to yield the thinnest possible passband. In terms of materials, the dielectric materials containing in the optical filters include the titanium dioxide (TiO_2) and the silicon dioxide (SiO_2). These materials present refractive indexes in the visible spectrum of about 3.0 and ~1.5, respectively. Additionally, it is extremely difficult or even impossible to remove them from the substrate. The SiO_2 is a selected material because the refractive index in the visible range (e.g. in the band between 480 and 700 nm) is almost constant. The TiO_2 was selected due to fabrication constraints (the deposition process is well characterised) and because it is compatible with the silicon that forms the microelectronic circuits. The optical filters will be postprocessed by reactive plasma sputtering deposition of TFs on top of the photodetectors. The filter fabrication starts with the deposition of a TiO_2 layer after the completion of the standard CMOS process, including the removal overlayer (this issue will be further discussed). Then, the subsequent layers of SiO_2 and TiO_2 will be deposited with the suitable thicknesses. The Figure 4 illustrates the general structure of an individual optical filter, where it can be observed the existence of nine layers. The middle layer of the filters is composed by SiO_2, e.g., it is filled with the material with smaller index of refraction, and for this reason is denominated by ***L***. Additionally, the external layers (or mirrors) are composed by alternated layers of TiO_2 (the higher index of refraction, e.g., the ***H*** material) and SiO_2 layers. For this reason the *M* elementary structures that compose the mirrors are

denominated by ***HL*** (in the top mirror) and ***LH*** (in the bottom mirror). In conclusion and since the dielectric layers exist in odd numbers (e.g., N=2M+1 layers), the optical filter is composed by the following sequence of structures: $[(\boldsymbol{LH}\cdots\boldsymbol{LH})\boldsymbol{L}(\boldsymbol{HL}\cdots\boldsymbol{HL})]$ or $[(\boldsymbol{HL})^{M/2}\boldsymbol{L}(\boldsymbol{HL})^{M/2}]$. The example of the Figure 4 illustrates four Fabry-Perot interferometers composed by N=9 (M=4 and M/2=2) dielectric materials. The lengths of all cavities are different between them and are filled with the material relative to the ***L*** material (SiO_2). The top and bottom mirrors are equal in all interferometers and composed by M/2 ***HL*** (TiO_2/SiO_2) and M/2 ***LH*** (SiO_2/TiO_2) structures respectively.

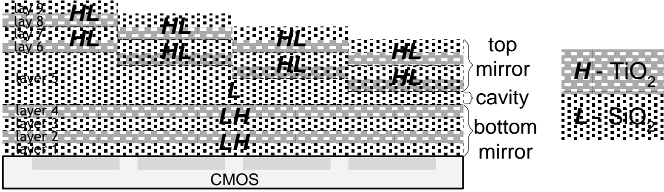

Figure 4: An example showing 4 optical filters with 2 mirrors (each one composed by 4 layers and 2 ***HL***/***LH*** structures) and 4 cavities (***L*** material) to allow only 4 wavelengths to pass from the top into the bottom direction.

A set of sixteen optical filters with its own central frequency was designed for a reasonable full cover of the visible range. All the ***HL*** and ***LH*** structures present the same thickness, whose individual thicknesses are 85 nm and 57 nm for the materials composed by SiO_2 (***L*** material) and TiO_2 (***H*** material), respectively. The only difference relies in the middle layer, e.g., in the cavity's thickness of each optical filter. The thicknesses of each layer of all optical filters and the respective central wavelength (located in the wavelength that present the larger transmittance) are listed in the Table II.

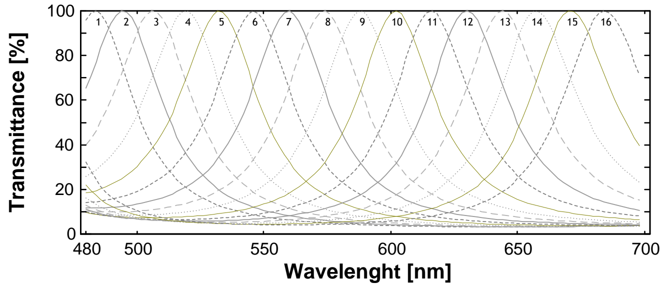

(a)

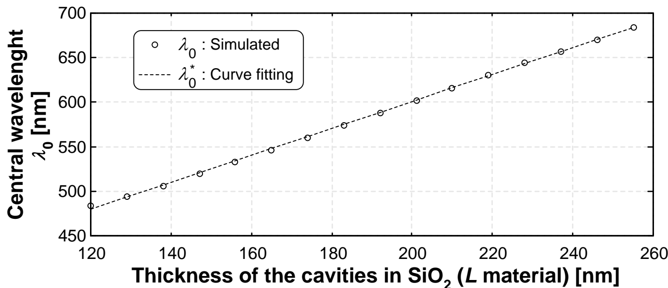

(b)

Figure 5: (a) Simulated transmittance versus the wavelength for a set of 16 optical filters with mirrors made of dielectric materials. Each top/bottom mirror is composed by two ***HL***/***LH*** structures made of ***H*** (TiO_2) and ***L*** (SiO_2) materials with thicknesses of 57 nm and 85 nm, respectively. The middle layers (e.g., the cavities) are made of ***L*** materials (SiO_2) and present thicknesses in the 120-255 nm wavelength range that varies in integer steps of 9 nm. (b) Central wavelength λ_0 [nm] versus the cavities' thicknesses [nm] and an equation giving $\lambda_0^*=\lambda_0^*(th)$ in terms of the cavity's thickness, which were obtained by applying the minimum squares methods into $\lambda_0=\lambda_0(th)$.

The Figure 5(a) shows the simulated transmittances [%] versus the wavelength [nm] in the visible range, whereas the Figure 5(b) shows the behavior of the central frequencies λ_0 [nm] in terms of the cavity thickness th [nm]. A simple closed form equation defining the central wavelength λ_0^* in terms of the cavity's thickness can be obtained by applying the minimum square method into the simulated data. The curve fitting is represented in by a dashed in the Figure 5(b) and is defined by:

$$\lambda_0^* = 299 + 1.51 \times th \qquad (1)$$

The line λ_0^* agrees well with the simulated central wavelengths λ_0 due to the high correlation coefficient ρ=99.99%.

In terms of design, the thicknesses of the individual cavities were selected on 9 nm steps to make easy their precise definition. In the Figure 6 is possible to observe the concept behind the fabrication, which is based in the thinning of the SiO_2 layers into sixteen channels with different thicknesses. In the first step, all cavities are deposited with the same thickness. Then, four corrosion masks can be used for achieving the final thickness of each cavity. The black squares in white masks represent holes for allowing the plasma etching of the SiO_2.

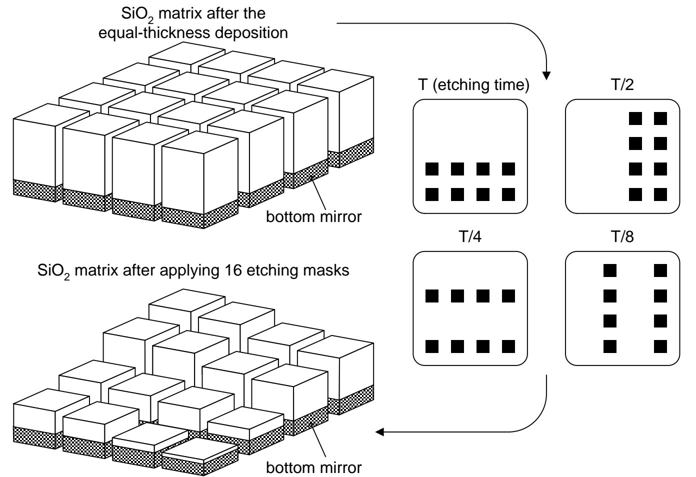

Figure 6: The principle to form the individual cavities. After the first step with the deposition of 16 cavities with equal thicknesses, different etching times are used for each one of the etching masks. The result is a SiO_2 matrix with different thicknesses.

D. *CMOS photodetectors*

An imager array with photodetectors was fabricated for light-current conversion. The photodetectors are based on N^+/P-substrate junction photodiode fabricated in a CMOS process, because it provides the best spectral responsivity in the desired spectral range of photodiodes available in a CMOS process and yields the highest possible fill-factor, since a deep N-well is not required for every pixel.

Table II: The thicknesses of the 9 dielectric layers that form the optical filters (OFs) illustrated in the Figure 4.

λ_0 [nm]	Layer number [#]								
	1	2	3	4	5	6	7	8	9
	Thickness [nm]								

484	85	57	85	57	120	57	85	57	85
494	85	57	85	57	129	57	85	57	85
506	85	57	85	57	138	57	85	57	85
520	85	57	85	57	147	57	85	57	85
533	85	57	85	57	156	57	85	57	85
546	85	57	85	57	165	57	85	57	85
560	85	57	85	57	174	57	85	57	85
574	85	57	85	57	183	57	85	57	85
588	85	57	85	57	192	57	85	57	85
602	85	57	85	57	201	57	85	57	85
616	85	57	85	57	210	57	85	57	85
630	85	57	85	57	219	57	85	57	85
644	85	57	85	57	228	57	85	57	85
657	85	57	85	57	237	57	85	57	85
670	85	57	85	57	246	57	85	57	85
684	85	57	85	57	255	57	85	57	85

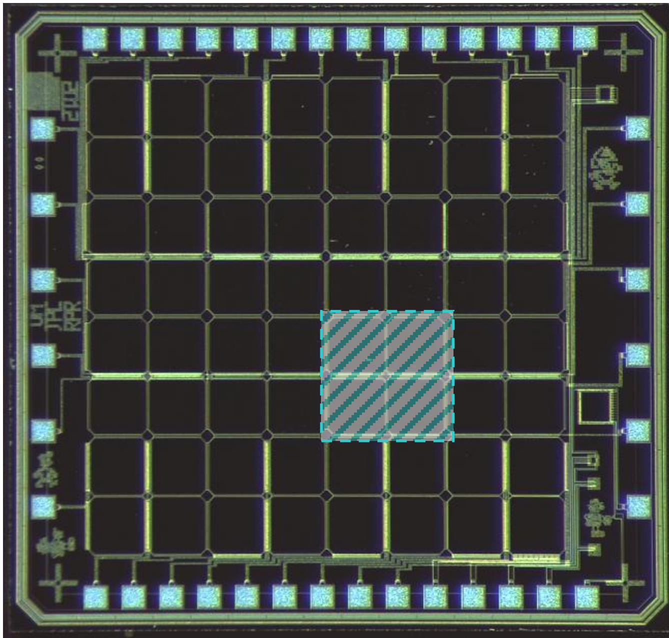

Figure 7: A photograph showing the CMOS microdevice prototype. The shaded part illustrates how groups of 2×2 photodiodes are tied together to form a compound photodetector for each of the 16 wavelength channels.

It was selected the on-semicondutor 2-metals/1-poly 0.7μm CMOS process for fabricating a photodetectors array. In this CMOS process, the junction depth of the photodiodes is fully defined and cannot be changed. However, the spectral responsivity (the sensitivity) can be improved by a suitable arrangement of dielectric layers on top of the photodiode surface. In this CMOS process there are three major dielectric layers above the PN junction that implements the photodetector. Nonetheless, the top layer (overlayer) is made of silicon nitride. In spite to be against the wise use of the design rules, the on-semiconductor foundry allows the overlayer removable without providing any metal layer bellow. The Figure 7 shows a photograph of the fabricated CMOS microdevice prototype with a photodetectors array composed by a matrix of 8×8 photodiodes. It must be noted that groups of 2×2 photodiodes (each one with its microlens) were tied together to form a matrix of 16 compound photodetectors.

III. EXPERIMENTAL

A. Microlenses

The subjective evaluation of the optical quality of microlenses was done by impinging a laser beam (generated from a neon source) into the array and observing the diffraction pattern into a white plane. As showed in the Figure 8, the subjective quality of the microlenses array is very good. It can also be observed in the Figure 8 that each lens in the array spreads the laser beam into a specific direction. Moreover, it is possible to observe the interaction between the spreaded beams. The structural and optical quality that were observed during the process optimization and during the characterization of the microlenses arrays open good perspectives for fabricating stereoscopic image sensors at low cost.

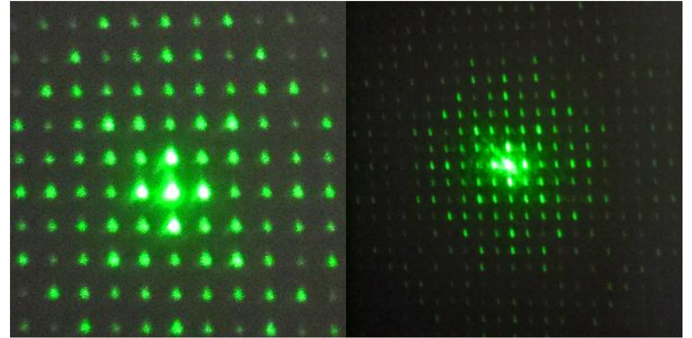

Figure 8: Photographs with projections of few laser beams after being spread from the impinging one by the array of microlenses. It is possible to note interference patterns between beams, especially in the middle.

B. CMOS photodetectors

The Figure 9 shows few photographs of the experimental setup that was used for characterizing the compound photodetectors. This setup is composed by a dark chamber, a digitally-controlled LED-based light source (with the respective control circuits), a transresistance amplification interface board, a metallic positioning/aligning mechanical support and by a CMOS microdevice (encapsulated with a DIP packaging) similar to this one showed in the Figure 7. The dark chamber prevents interferences from the environmental light to impinge into the photodetectors, whereas a personal computer running the LabView software and an Arduino board (with analog inputs and digital outputs) controls both the acquisition process and the intensity regulation of the light source. The Figure 9(a) shows the Arduino board attached to a second board (the analog board) with a socket to allow the connection of any type of microdevice. In fact, an adaptation board (similar to those one showed) is required to respect the pinout sequence of the analog board. It can also be observed that the window of the CMOS microdevice is opened for allowing the light to impinge the photodetectors. The analog board contains sixteen transresistance amplifiers (Burr-Brown's OPA413UA reference IC) whose outputs connects simultaneously to the sixteen analog inputs of the Arduino board for maximizing the acquisition speed and at the same time reducing the complexity of control. The light source uses an analog signal to control the light's intensity, therefore, eight digital outputs of the Arduino were used by LabView to select the intensity on equal steps with the help of a 8-bits digital-to-analog converter in the DAC board. The Figure 9(b) shows a personal computer (PC) running the LabView

application and communicating with the Arduino board through a USB cable. It is also possible to observe both the adaptation and analog boards, as well as the CMOS microdevice under illumination. The Figure 9(c) shows a detailed view of the Arduino board and both the back (in the left part of the photograph) and the front (right) views of the analog board. A detailed view of the adaptation board and the CMOS microdevice can also be observed in this same Figure.

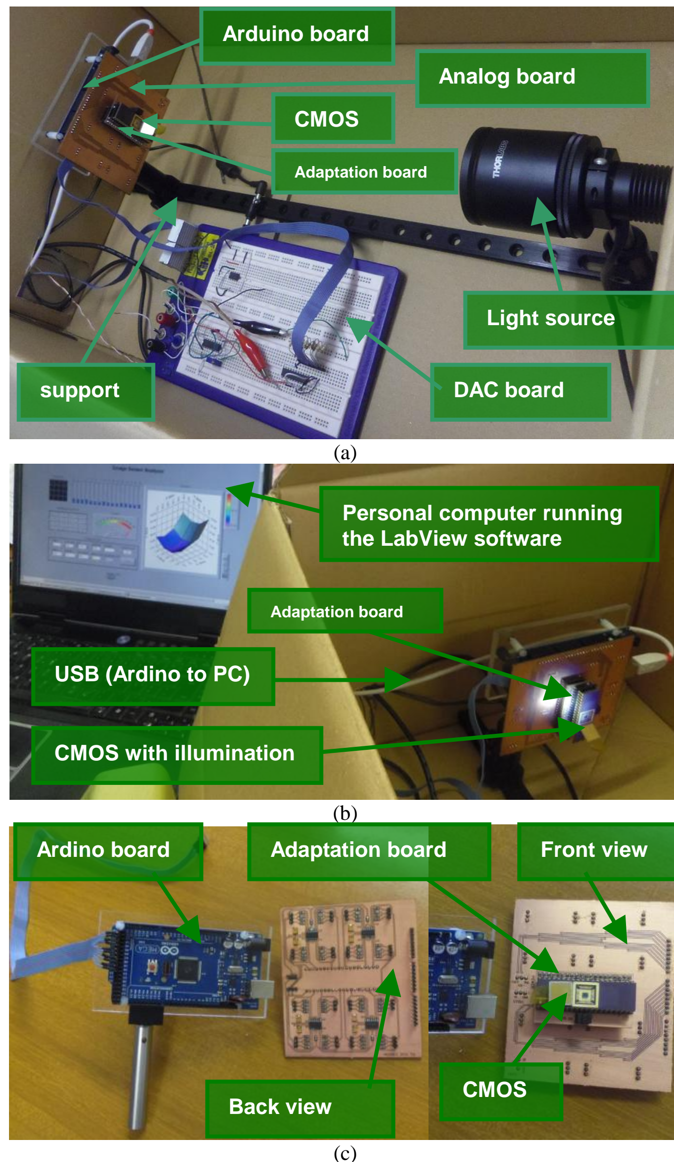

Figure 9: For the photographs of the setup that was used to characterize the compound photodetectors: (a) general view inside the dark chamber; (b) personal computer and LabView application responsible for controlling the acquisition process; and (c) back (left) and front (right) closed up views of the analog board with a matrix of 16 selectable transresistance amplifiers.

The plot depicted in the Figure 10 shows the mean value of the photocurrent [nA] behaviour that was measured in terms of the intensity [lux] of the light source.

IV. Conclusions

This paper presented an optical sensor based on Fabry Perot interferometry for spectroscopy in the visible region (e.g., from 480 to 700 nm) of the electromagnetic spectrum.

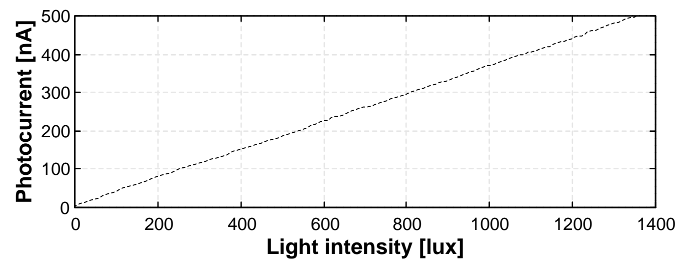

Figure 10: Measured [mean value] behavior of the compound photodetectors.

Acknowledgements

This work and the postdoctoral scholarchip of Doctor Yuri Andrey Olivato Assagra were both sponsored by the Brazilian agency National Council of Scientific Research (CNPq) under the grant 400110/2014-8. Talita Conte Granado was also supported by a scholarship granted by the CNPq agency.

References

[1] J. P. Carmo, L. M. Gonçalves, and J. H. Correia, “Multi-chip-module-based micropyrometer with an IR metamaterials lens and bandpass optical filter", in. Proc. 4th International Conference MetaMaterials 2009, London, UK, 30 Aug- 4 Sept. 2009, pp. 722-724.

[2] J. P. Carmo, R. P. Rocha, M. Bartek, *et al.*, "A review of visible-range Fabry–Perot microspectrometers in silicon for the industry", Journal of Optics & Lasers Technolongy: Elseviser Science, Vol. 44, No. 7, pp. 2312-2320, October 2012.

[3] G. Barbera, G. Barone, V. Crupi, *et al.*, “Nondestructive analyses of carbonate rocks: applications and potentiality for museum materials”, X-Ray Spectrometry, Vol. 42, No. 1, pp. 8-15, January/February 2013.

[4] M. Z. Mesmer, and R. D. Satzger, “Determination of anabolic steroids by HPLC with UV-vis-particle beam mass spectrometry”, Journal of Chromatography Science, Vol. 35, No. 1, pp. 38-42, 1997.

[5] J. P. Carmo, and J. E. Ribeiro, “Optical techniques for defect evaluation in vehicles”, Chapter #10 in the book New Advances in Vehicular Technology and Automotive Engineering: Edited by J. P. Carmo and J. E. Ribeiro, InTech Open Science, ISBN 978-953-51-0698-2, 1st August 2012, pp. 255-282.

[6] G. M. Yee, N. I. Maluf, P. A. Hing, *et al.*, "Miniature spectrometers for biochemical analysis", Sensors and Actuators A, Vol. 58, No. 1, pp. 61-66, January 1997.

[7] J. Xing, M. Ngadi, A. Gunenc, *et al.*, “Use of visible spectroscopy for quality classification of intact pork meat”, Journal of Food Engineering, Vol. 82, No. 2, Pp. 135-141, September 2007.

[8] D. Brennan, J. Alderman, L. Sattler, *et al.*, "Issues in development of NIR micro spectrimeter system for on-line process monitoring of milk product", Measurement, Vol. 33, pp. 67-74, 2003.

[9] T. Bifano, “MEMS deformable mirrors”, Nature Photonics, Vol. 5, pp. 21-23, January 2011.

[10] K. Kitamura, T. Watanabe, T. Sawamoto, *et al.*, "A 33-megapixel 120-frames-per-second 2.5-Watt CMOS image sensor with column-parallel two-stage cyclic analog-to-digital converters", IEEE Transactions on Electron Devices, Vol. 59, No. 12, pp. 3426-3433, December 2012.

[11] C.-D. Liao, and J.-C. Tsai, "The evolution of MEMS displays", IEEE Transactions on Industrial Electronics, Vol. 56, No. 4, pp. 1057-1065, April 2009.

View publication stats